Intrinsic alignment of simulated galaxies in the cosmic web: implications for weak lensing surveys

S. Codis, R. Gavazzi, Y. Dubois, C. Pichon, K. Benabed, V. Desjacques, D. Pogosyan, J. Devriendt, A. Slyz

Monthly Notices
of the
ROYAL ASTRONOMICAL SOCIETY

MNRAS **448,** 3391–3404 (2015) doi:10.1093/mnras/stv231

Intrinsic alignment of simulated galaxies in the cosmic web: implications for weak lensing surveys

S. Codis,[1,2]★ R. Gavazzi,[1,2] Y. Dubois,[1,2] C. Pichon,[1,2] K. Benabed,[1,2] V. Desjacques,[3] D. Pogosyan,[4] J. Devriendt[5] and A. Slyz[5]

[1]*CNRS, UMR7095, Institut d'Astrophysique de Paris, 98 bis Boulevard Arago, F-75014 Paris, France*
[2]*Sorbonne Universités, UPMC Univ. Paris 06, UMR7095, Institut d'Astrophysique de Paris, 98 bis Boulevard Arago, F-75014 Paris, France*
[3]*Département de Physique Théorique, Université de Genève, 24 quai Ernest Ansermet, CH-1211 Genève, Switzerland*
[4]*Department of Physics, University of Alberta, 11322-89 Avenue, Edmonton, Alberta T6G 2G7, Canada*
[5]*Sub-department of Astrophysics, University of Oxford, Keble Road, Oxford OX1 3RH, UK*

Accepted 2015 February 3. Received 2015 January 30; in original form 2014 June 18

ABSTRACT

The intrinsic alignment of galaxy shapes (by means of their angular momentum) and their cross-correlation with the surrounding dark matter tidal field are investigated using the 160 000, $z = 1.2$ synthetic galaxies extracted from the high-resolution cosmological hydrodynamical simulation HORIZON-AGN. One- and two-point statistics of the spin of the stellar component are measured as a function of mass and colour. For the low-mass galaxies, this spin is *locally* aligned with the tidal field 'filamentary' direction while, for the high-mass galaxies, it is *perpendicular* to both filaments and walls. The bluest galaxies of our synthetic catalogue are more strongly correlated with the surrounding tidal field than the reddest galaxies, and this correlation extends up to $\sim 10\,h^{-1}$ Mpc comoving distance. We also report a correlation of the projected ellipticities of blue, intermediate-mass galaxies on a similar scale at a level of 10^{-4} which could be a concern for cosmic shear measurements. We do not report any measurable intrinsic alignments of the reddest galaxies of our sample. This work is a first step towards the use of very realistic catalogue of synthetic galaxies to evaluate the contamination of weak lensing measurement by the intrinsic galactic alignments.

Key words: gravitational lensing: weak – methods: numerical – cosmology: theory – large-scale structure of Universe.

1 INTRODUCTION

For the last two decades, weak gravitational lensing has emerged as one of the most promising cosmological probes of the dark matter and dark energy contents of the Universe, culminating in the design of several large surveys like Dark Energy Survey (DES),[1] *Euclid* (Laureijs et al. 2011) or Large Synoptic Survey Telescope (LSST).[2]

As the statistical power of weak lensing surveys is ramping up, more and more attention has to be paid for the control of systematic effects. Among the critical astrophysical sources of errors is the problem of the intrinsic alignments (IA) of galaxies. The fundamental assumption upon which galaxies are randomly aligned in the absence of a shear signal that is coherent on the scales of several arcminutes is likely to break down for pairs of galaxies observed at close angular distances (through direct gravitational interactions or as a result of the same local tidal field they live in). Much effort has thus been made to control the level of IA of galaxies as a potential source of systematic errors in weak gravitational lensing measurements (e.g. Croft & Metzler 2000; Heavens, Refregier & Heymans 2000; Hirata & Seljak 2004), although some techniques have been proposed to mitigate their nuisance by making extensive use of photometric redshifts (e.g. Bridle & King 2007; Joachimi & Schneider 2008, 2010; Joachimi & Bridle 2010; Kirk, Bridle & Schneider 2010; Blazek et al. 2012).

Direct measurements of the alignment of the projected light distribution of galaxies in wide field imaging data seem to agree on a contamination at a level of a few per cent in the shear correlation functions, although the amplitude of the effect depends on the depth of observations (stronger for shallower surveys), the amount of redshift information and the population of galaxies considered (in the sense that red galaxies seem to show a strong intrinsic projected shape alignment signal whereas observations only place upper limits in the amplitude of the signal for blue galaxies; Bernstein & Norberg 2002; Brown et al. 2002; Lee & Pen 2002; Heymans et al. 2004; Hirata et al. 2004, 2007; Mandelbaum et al. 2006, 2011; Joachimi et al. 2011, 2013a). Direct observations of the alignment between the spin and the tidal tensor eigenvectors have also been

★ E-mail: codis@iap.fr
[1] http://www.darkenergysurvey.org
[2] http://www.lsst.org

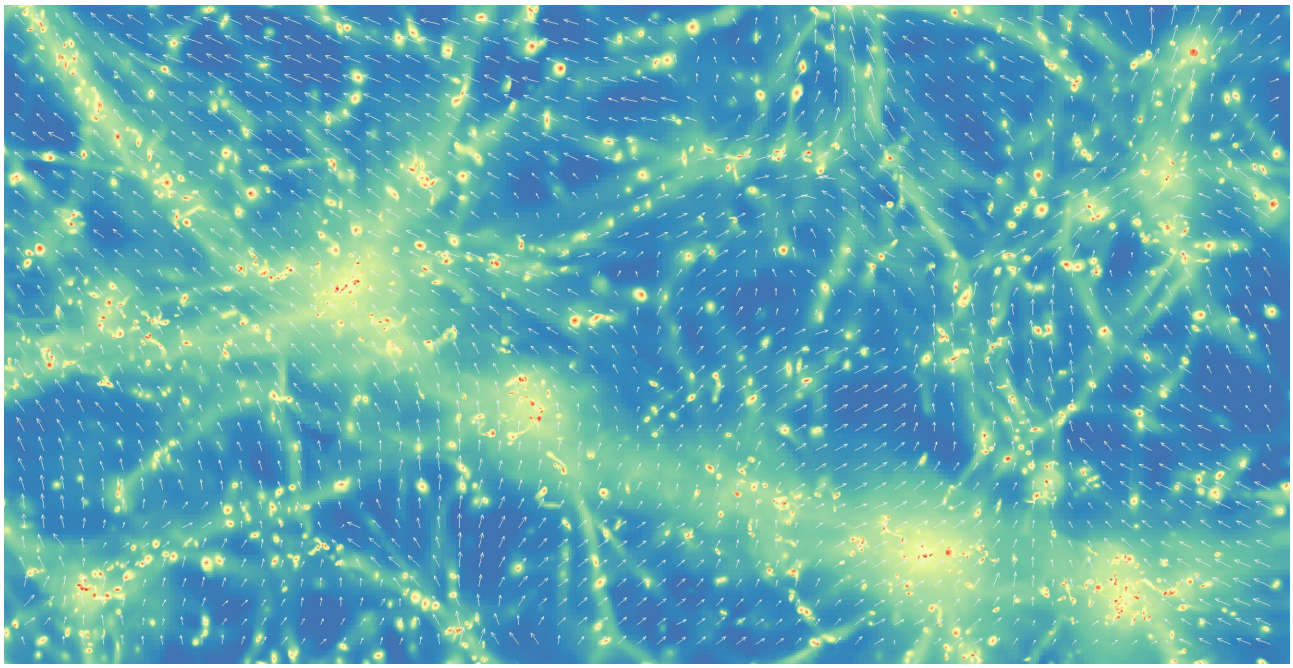

Figure 1. The $\boldsymbol{e}_1$ eigenvector (white arrows) of the tidal field within a slice of 25 h^{-1} Mpc comoving in depth and 12.5 h^{-1} Mpc comoving horizontally together with the gas density (from blue to red) within the HORIZON-AGN simulation at $z = 1.2$. As expected, $\boldsymbol{e}_1$ statistically follows the filaments.

carried out: the first attempt by Lee & Pen (2002) studied the correlations between the disc orientation of the galaxies from the Tully catalogue and the shear reconstructed from the Point Source Catalogue Redshift Survey and confidently rejected the hypothesis of randomness. More recently, Lee et al. (2013) detected some correlations between the spin and the intermediate eigenvector of the tidal tensor and found that galactic spins were also preferentially perpendicular to the major principal axis but this signal remains weak.

Cosmological numerical simulations are a natural way of further refining our models of IA. The imprint of the large-scale dynamics on to the shapes and spins of galaxies has been extensively studied using dark matter (DM) simulations (Aubert, Pichon & Colombi 2004; Bailin & Steinmetz 2005; Aragón-Calvo et al. 2007; Hahn et al. 2007b; Lee et al. 2008; Paz, Stasyszyn & Padilla 2008; Sousbie et al. 2008; Codis et al. 2012; Laigle et al. 2015; Forero-Romero, Contreras & Padilla 2014, among others). One can also mention a numerical study of the alignment between halo spin and tidal tensor by Porciani, Dekel & Hoffman (2002), who predicted its orthogonality with the major principal axis but also found that galactic spins must have lost their initial alignment with the tidal tensor predicted by tidal-torque theory (TTT), and by Codis et al. (2012). However, given the complex dependency on the physical properties of the galaxies seen in the observation, it is probably difficult to rely on DM-only numerical simulations as the sole resort to predict and control IA for weak lensing applications despite some success with the addition of halo model or semi-analytical models (e.g. Schneider & Bridle 2010; Joachimi et al. 2013b).

The advent of hydrodynamical cosmological simulations is arguably the best way forward to make better predictions on the complex relation between halo shape and spin and galaxy shape and spin. Local studies of the relation between DM and baryonic spins or inertia tensors have been conducted to measure the degree of alignment between the inertia tensor of the DM halo and the stellar component (not weighted by luminosity; Hahn, Teyssier & Carollo 2010; Tenneti et al. 2014). They find a typical excursion of the misalignment angle of 30°–10° for haloes ranging in mass from 10^{10} to $10^{14}\,h^{-1}\,\mathrm{M}_{\odot}$.

More recently, Dubois et al. (2014) measured the alignment of galaxy spins with the large-scale filamentary network in the HORIZON-AGN simulation, a state-of-the-art hydrodynamical simulation which produced synthetic galaxies displaying morphological diversity by redshift $z = 1.2$. Dubois et al. found that simulated galaxies have a spin which is either parallel to their neighbouring filament for low-mass, disc-dominated blue galaxies, or perpendicular to it for high-mass, velocity-dispersion-dominated red galaxies, the rapid reorientation of the latter massive galaxies being due to mergers. This suggests a scenario in which galaxies form in the vorticity-rich neighbourhood of filaments, and then migrate towards the nodes of the cosmic web, converting their orbital momentum into spin. The inherently anisotropic nature of the large-scale structure (filaments and walls) and its complex imprint on the shape and spin of galaxies (see also Pichon et al. 2014) may prevent isotropic approaches from making accurate predictions and suggest that the imprint of IA might be more severe for higher order statistics of the cosmic shear signal and definitely not addressable with simple prescriptions for the relation between the spin or inertia tensor of haloes and galaxies.

We thus propose here to extend the work of Dubois et al. (2014) by bringing the findings of the HORIZON-AGN simulation (see Fig. 1) closer to the framework of weak lensing observables. In particular we will measure the correlations between galactic spins and their surrounding tidal field (related to the so-called GI term of Hirata & Seljak 2004) and the correlations between spins themselves (related to the so-called II term of the same reference). We will also exhibit the variation of this quantity with the mass and colour of our galaxies, looking for populations where the IA effect is particularly severe or reduced. Our main finding is an excess alignment between the bluest galaxies of our synthetic catalogue, and no detectable alignment for the reddest ones. This conclusion

is in apparent contradiction with the works cited above, and we will discuss how this can be explained mainly by selection effects (on mass range, redshifts of catalogue, etc.).

Throughout this work, we use the stellar spin as a proxy for the ellipticity of galaxies, without attempting to project galactic ellipticities perpendicular to a given sightline. This choice differs from other authors who rather considered the inertia tensor of the stellar mass (see e.g. Tenneti et al. 2014). We believe spin can give a complementary insight on the apparent luminosity-weighted projected morphology of a generally star-forming galaxy. In addition, as one gets closer to the resolution limit of the simulation, we believe that the reliability of the simulated spin will hold longer than the reliability of the overall shape of the stellar component. Although we mainly focus on 3D quantities that are better suited to quantify the physical degree of IA in our simulation, we give some guidelines for inferring projected quantities, in the usual formalism of weak lensing.

The paper is organized as follows. Section 2 presents the HORIZON-AGN simulation and describes our method for measuring spin and inertia tensor. It also illustrates how much the shape inferred from spin can be favourably compared to the shape inferred from the inertia tensor of stars, hence supporting our choice of using the spin as a proxy for the ellipticity of galaxies. Section 3 defines how intrinsic alignments are quantified and where they contaminate the weak lensing observables. In Section 4, we present the cross-correlation between the principal axes of the tidal tensor and the spin vector as a function of distance and further show the zero-lag one-point probability distribution function (PDF) of this angle. Section 5 investigates the spin–spin two-point correlation as a function of separation and the projected ellipticity two-point correlation function. Section 6 checks that grid locking effects do not dominate the measurements. We finally conclude in Section 7 and discuss briefly how the statistics depends on the synthetic colours of galaxies. We also sketch how our findings can be cast into predictions on the contamination of weak lensing by IA. Appendix A studies the corresponding alignments for DM haloes.

2 THE SYNTHETIC UNIVERSE

Let us shortly describe the HORIZON-AGN simulation (Section 2.1; see Dubois et al. 2014 for more details) and explain how galaxy properties are extracted out of it (Section 2.2).

2.1 The HORIZON-AGN simulation

A standard Λ cold dark matter (ΛCDM) cosmology compatible with the 7-year *Wilkinson Microwave Anisotropy Probe* (*WMAP*-7) cosmology (Komatsu et al. 2011) is adopted, with total matter density $\Omega_\mathrm{m} = 0.272$, dark energy density $\Omega_\Lambda = 0.728$, amplitude of the matter power spectrum $\sigma_8 = 0.81$, baryon density $\Omega_\mathrm{b} = 0.045$, Hubble constant $H_0 = 70.4\,\mathrm{km\,s^{-1}\,Mpc^{-1}}$ and $n_\mathrm{s} = 0.967$. The HORIZON-AGN simulation has been run with 1024^3 DM particles in a $L_\mathrm{box} = 100\,h^{-1}$ Mpc box, so as to obtain a DM mass resolution of $M_\mathrm{DM,res} = 8 \times 10^7\,\mathrm{M}_\odot$. The adaptive mesh refinement (AMR) code RAMSES (Teyssier 2002) has been used to run the simulation with an initial mesh refinement of up to $\Delta x = 1$ kpc (seven levels of refinement). The refinement scheme follows a quasi-Lagrangian criterion: if the number of DM particles in a cell is more than eight, or if the total baryonic mass in a cell is eight times the initial DM mass resolution, a new refinement level is triggered.

A Sutherland & Dopita (1993) model is used to allow gas cooling by means of H and He cooling down to 10^4 K with a contribution from metals. Following Haardt & Madau (1996), heating from a uniform ultraviolet (UV) background takes place after redshift $z_\mathrm{reion} = 10$. We model metallicity as a passive variable for the gas that varies according to the injection of gas ejecta during supernovae explosions and stellar winds. A Schmidt law is used to model star formation: $\dot{\rho}_* = \epsilon_* \rho / t_\mathrm{ff}$, where $\dot{\rho}_*$ is the star formation rate density, $\epsilon_* = 0.02$ (Kennicutt 1998; Krumholz & Tan 2007) the constant star formation efficiency and t_ff the local free-fall time of the gas. We allow star formation where the gas hydrogen number density exceeds $n_0 = 0.1\,\mathrm{H\,cm^{-3}}$ according to a Poisson random process (Rasera & Teyssier 2006; Dubois & Teyssier 2008) with a stellar mass resolution of $M_{*,\mathrm{res}} = \rho_0 \Delta x^3 \simeq 2 \times 10^6\,\mathrm{M}_\odot$.

We model stellar feedback using a Salpeter (1955) initial mass function with a low-mass (high-mass) cut-off of $0.1\,\mathrm{M}_\odot$ ($100\,\mathrm{M}_\odot$). In particular, the mechanical energy from Type II supernovae and stellar winds follows the prescription of STARBURST99 (Leitherer et al. 1999, 2010), and the frequency of Type Ia supernovae explosions is taken from Greggio & Renzini (1983).

Active galactic nuclei (AGN) feedback is modelled according to Dubois et al. (2012). A Bondi–Hoyle–Lyttleton accretion rate on to black holes is used $\dot{M}_\mathrm{BH} = 4\pi\alpha G^2 M_\mathrm{BH}^2 \bar{\rho} / (\bar{c}_\mathrm{s}^2 + \bar{u}^2)^{3/2}$, where M_BH is the black hole (BH) mass, $\bar{\rho}$ is the average gas density, $\bar{c}_\mathrm{s}$ is the average sound speed, $\bar{u}$ is the average gas velocity relative to the BH velocity and α is a dimensionless boost factor with $\alpha = (\rho/\rho_0)^2$ when $\rho > \rho_0$ and $\alpha = 1$ otherwise (Booth & Schaye 2009) in order to account for our inability to capture the colder and higher density regions of the interstellar medium. The effective accretion rate on to BHs is capped at the Eddington accretion rate: $\dot{M}_\mathrm{Edd} = 4\pi G M_\mathrm{BH} m_\mathrm{p} / (\epsilon_\mathrm{r} \sigma_\mathrm{T} c)$, where σ_T is the Thompson cross-section, c is the speed of light, m_p is the proton mass and ϵ_r is the radiative efficiency, assumed to be equal to $\epsilon_\mathrm{r} = 0.1$ for the Shakura & Sunyaev (1973) accretion on to a Schwarzschild BH. Two different modes of AGN feedback are accounted for, the *radio* mode operating when $\chi = \dot{M}_\mathrm{BH} / \dot{M}_\mathrm{Edd} < 0.01$ and the *quasar* mode active otherwise. More details are given in Dubois et al. (2014).

2.2 Data analysis

2.2.1 *Galaxy catalogue*

Galaxies are identified with the ADAPTAHOP finder (Aubert et al. 2004), which relies directly on the distribution of star particles to construct the catalogue of galaxies. 20 neighbours are used to compute the local density of each particle. A local threshold of $\rho_\mathrm{t} = 178$ times the average total matter density is applied to select relevant densities. Note that the galaxy population does not depend sensitively on the exact value chosen for this threshold. Our specific choice reflects the fact that the average density of galaxies located at the centre of galaxy clusters is comparable to that of their host. The force softening (minimum size below which substructures are treated as irrelevant) is of $\sim$10 kpc. Only galactic structures identified with more than 50 star particles are included in the mock catalogues. This enables a clear identification of galaxies, including those in the process of merging. A galaxy catalogues with $\sim$165 000 objects is produced at $z = 1.2$ with masses between 1.7×10^8 and $1.4 \times 10^{12}\,\mathrm{M}_\odot$. The galaxy stellar masses quoted in this paper should be understood as the sum over all star particles that belong to a galaxy structure identified by ADAPTAHOP. Note that most results are derived from a subsample of galaxies with a mass above $10^9\,\mathrm{M}_\odot$, which corresponds to 300 stellar particles.

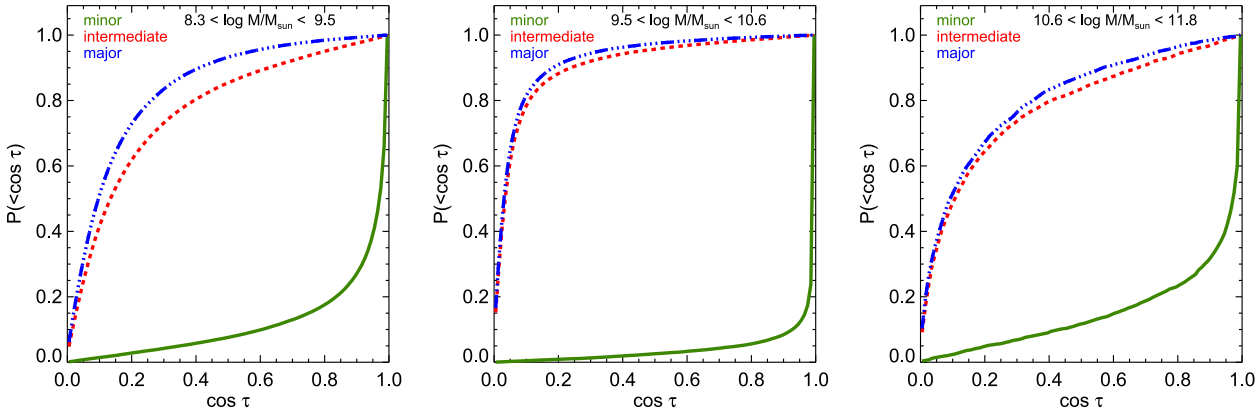

Figure 2. Cumulative PDF of the cosine of the angle, $\cos\tau$, between the galaxy spin and the minor (green solid), intermediate (red dashed) and major (blue dot–dashed) axis of the inertia tensor of the galaxy at $z = 1.2$. Galaxies tend to align their spin with the minor axis. The most massive galaxies, which are more likely dominated by dispersion rather than rotation, show less correlation.

2.2.2 *Spin and shape of galaxies*

To assign a spin to the galaxies, we compute the total angular momentum of the star particles which make up a given galactic structure relative to the particle of maximum density (centre of the galaxy). To identify the latter, we use the smoothed stellar density constructed with the ADAPTAHOP algorithm. We can therefore write the intrinsic angular momentum vector $\boldsymbol{L}$ or spin of a galaxy as

$$\boldsymbol{L} = \sum_{\alpha=1}^{N} m^{(\alpha)} \boldsymbol{x}^{(\alpha)} \times \boldsymbol{v}^{(\alpha)}, \tag{1}$$

where the superscript α denotes the αth stellar particle of mass $m^{(\alpha)}$, position $\boldsymbol{x}^{(\alpha)}$ and velocity $\boldsymbol{v}^{(\alpha)}$ relative to the centre of mass of that galaxy. Likewise, we also measure the (reduced) inertia tensor of a galaxy:

$$I_{ij} = \frac{\sum_{\alpha=1}^{N} m^{(\alpha)} x_i^{(\alpha)} x_j^{(\alpha)}}{\sum_{\alpha=1}^{N} m^{(\alpha)}}. \tag{2}$$

This inertia tensor is then diagonalized to obtain the eigenvalues $\lambda_1 \leq \lambda_2 \leq \lambda_3$ and the corresponding unit eigenvectors $\boldsymbol{u}_1$, $\boldsymbol{u}_2$ and $\boldsymbol{u}_3$ (respectively minor, intermediate and major axis of the ellipsoid).

Fig. 2 shows the PDF of the angle τ_i between the spin and each of the principle axes $\boldsymbol{u}_i$ of the galaxies:

$$\cos\tau_i = \frac{\boldsymbol{L}\cdot\boldsymbol{u}_i}{|\boldsymbol{L}|}. \tag{3}$$

As expected, galaxies tend to have a spin well aligned with the minor axis ($\boldsymbol{u}_1$) of the inertia tensor, with a mean value $\langle\cos\tau_1\rangle = 0.90$. The correlation is slightly less pronounced for the most massive galaxies, for which the rotation support is weaker compared to velocity dispersion, but it still shows a strong degree of alignment ($\langle\cos\tau_1\rangle = 0.85$).

Owing to the tight alignment between the spin of galaxies and the minor axis of the inertia tensor, we expect that an analysis of galactic spin or inertia tensor orientations will capture the physical mechanisms producing IA equally well. For weak lensing predictions, however, we shall pay attention to the modulus of the ellipticity and not only its direction when turning spins into projected ellipticities. Namely, the projected ellipticity of an axisymmetric discy galaxy depends on the disc thickness (e.g. Joachimi et al. 2013a,b). If we note q_d, the disc flattening or axis ratio, the apparent axis ratio q_p of a projected galaxy along the line of sight aligned with the z-axis, reads

$$q_\mathrm{p} = \frac{|L_z|}{|\boldsymbol{L}|} + q_\mathrm{d}\sqrt{1 - \frac{L_z^2}{|\boldsymbol{L}|^2}}. \tag{4}$$

In principle, we could measure the flattening of the simulated galaxies to infer the projected axis ratios. Unfortunately, the finite $1\,h^{-1}$ kpc resolution of the HORIZON-AGN simulation overestimates the thickness of the disc of low-mass galaxies. To alleviate this problem, we will assume $q_\mathrm{d} = 0$ in the remainder of this work, and thus maximize the moduli of the projected ellipticities. This can be seen as a conservative approach since we effectively maximize the implication of spin IA on apparent alignments of projected ellipticities, either for the correlation between spins themselves (II) or between spins and tidal tensor (GI). We shall come back to the fidelity of our simulations at recovering the eigenvalues of the inertia tensor and not only its eigendirections in a future work.

2.2.3 *Rest-frame intrinsic colours*

In order to ascertain the sensitivity of our measurements to galaxy colours, we compute the absolute AB magnitudes and rest-frame colours of the mock galaxies using single stellar population models from Bruzual & Charlot (2003) adopting a Salpeter initial mass function. Each star particle contributes a flux per frequency that depends on its mass, age and metallicity. The sum of the contribution of all star particles is passed through u, g, r or i filter bands from the Sloan Digital Sky Survey (SDSS). Fluxes are expressed as rest-frame quantities (i.e. that do not take into account the redshifting of spectra) and, for the sake of simplicity, dust extinction is neglected. Once all the star particles have been assigned a flux in each of the colour channels, we build the 2D projected maps for individual galaxies (satellites are excised with the galaxy finder). Summing up the contribution of their stars yields the galaxy luminosity in a given filter band.

Thorough this work, we will investigate the alignment properties of galaxies filtered by their colours. We separate our catalogue in three colour bins (in $u - r$) such that the number of galaxy in each is identical. Our bluest subset corresponds to $u - r < 0.78$ while the reddest one has $u - r > 1.1$. This choice insures a similar noise level in all of our measurements.

3 INTRINSIC ALIGNMENTS IN THE CONTEXT OF COSMIC SHEAR STUDIES

Weak lensing uses the apparent deformation of the shapes of galaxies on the sky to map the gravitational potential or measure its statistical properties like its power spectrum. The projected surface mass density, integrated along the line of sight to distant sources, is often preferred over the potential although they are trivially related by the Poisson equation. The effective convergence κ, which is nothing but the dimensionless projected density, is statistically described by its power spectrum $P_\kappa(\ell)$ as a function of wavenumber ℓ. For a source at comoving distance χ_s, we can write the convergence at an angular position $\boldsymbol{\theta}$ (Bartelmann & Schneider 2001):[3]

$$\kappa(\boldsymbol{\theta},\chi_s) = \frac{1}{c^2}\int_0^{\chi_s} \mathrm{d}\chi\, \frac{(\chi_s-\chi)\chi}{\chi_s}\left[\frac{\partial^2}{\partial x^2}+\frac{\partial^2}{\partial y^2}\right]\Phi,$$
$$= \frac{3H_0^2\Omega_0}{2c^2}\int_0^{\chi_s}\mathrm{d}\chi\,\frac{(\chi_s-\chi)\chi}{\chi_s}\frac{\delta(\chi\boldsymbol{\theta},\chi)}{a(\chi)}, \quad (5)$$

where χ is the comoving distance, a the expansion factor, δ the density contrast and Φ the three-dimensional gravitational potential are related by the Poisson equation:

$$\Delta\Phi = \frac{3H_0^2\Omega_0}{2a}\delta. \quad (6)$$

This can easily be generalized to a population of sources with a broad redshift distribution (Bartelmann & Schneider 2001).

The relation between Φ and δ can be cast into a relation between the lensing potential ϕ and effective convergence κ, and the effective shear γ_i, which involves the traceless parts of the projected tidal tensor. All these quantities are defined by

$$\phi = \frac{2}{c^2}\int_0^{\chi_s}\mathrm{d}\chi\,\frac{(\chi_s-\chi)\chi}{\chi_s}\Phi,\quad \kappa = \frac{1}{2}\left(\frac{\partial^2\phi}{\partial\theta_1^2}+\frac{\partial^2\phi}{\partial\theta_2^2}\right), \quad (7)$$

$$\gamma_1 = \frac{1}{2}\left(\frac{\partial^2\phi}{\partial\theta_1^2}-\frac{\partial^2\phi}{\partial\theta_2^2}\right),\quad \gamma_2 = \frac{\partial^2\phi}{\partial\theta_1\partial\theta_2}. \quad (8)$$

It is generally suitable to treat the shear in complex notations $\gamma = \gamma_1 + \mathrm{i}\gamma_2$. This quantity is most easily accessible as it captures the amount of anisotropic distortion a light bundle experiences on its way from a distant source to the observer. Therefore, the observed ellipticity of such a source, in the weak lensing regime of small distortions, is directly related to the shear. Indeed, by also defining a complex ellipticity $e = e_1 + \mathrm{i}e_2 = |e|e^{2\mathrm{i}\psi}$, such that $|e| = (1-q)/(1+q)$ and $q = b/a$ is the major (a) to minor (b) axis ratio, we have

$$e = e_s + \gamma, \quad (9)$$

where e is the apparent ellipticity and e_s the intrinsic source ellipticity (the one we would have observed without lensing).

An important statistics of this cosmic shear distortion field is the two-point correlation of projected ellipticities that can formally be split into the following components:

$$\langle e(\vartheta)e(\vartheta+\theta)\rangle_\vartheta = \langle e_s e_s'\rangle + 2\langle e_s\gamma'\rangle + \langle\gamma\gamma'\rangle, \quad (10)$$

where, for compactness, the prime means at an angular distance θ from the first location. The cosmological weak lensing signal is commonly decomposed into the ξ_+ and ξ_- shear correlation functions. Following Schneider et al. (2002), $\xi_\pm$ is given by

$$\xi_\pm(\theta) = \langle\gamma_+\gamma_+\rangle \pm \langle\gamma_\times\gamma_\times\rangle = \frac{1}{2\pi}\int_0^\infty \mathrm{d}\ell\,\ell P_\kappa(\ell)J_{0/4}(\ell\theta),$$

where J_0 and J_4 are the 0th- and 4th-order Bessel functions for ξ_+ and ξ_-, respectively. In this expression, γ_+ (respectively $\gamma_\times$) is the component of the complex shear orientated 0/90° (respectively ±45°) with respect to the line connecting two galaxies separated by a projected distance θ.

The fundamental assumption of weak lensing, which allows to infer shear properties from observed ellipticities, is that, on average, the intrinsic orientation of sources is completely random. The breakdown of this hypothesis yields additional terms to $\langle\gamma\gamma'\rangle$ on the right-hand side of equation (10) that have to be carefully accounted for in observations. The weak lensing signal is therefore contaminated by the two kinds of IA.

(i) The so-called 'II' term $\langle e_s e_s'\rangle$ induced by the intrinsic correlation of the shape of galaxies in the source plane (Croft & Metzler 2000; Heavens et al. 2000; Catelan, Kamionkowski & Blandford 2001). This mostly concerns pairs of galaxies that are at similar redshifts.

(ii) The so-called 'GI' term $\langle e_s\gamma'\rangle$ coming from correlation between the intrinsic ellipticity of a galaxy and the induced ellipticity (or shear) of a source at higher redshift (Hirata & Seljak 2004; Heymans et al. 2006; Joachimi et al. 2011). This non-trivial term is indirectly explained if the shape of galaxies is correlated with the local gravitational tidal field, which also contributes to the shear signal experienced by the far source in a given pair of observed ellipticities.

In this work we propose to measure these two effects in the HORIZON-AGN simulation, Section 4 being devoted to the 'GI' term (essentially captured by spin–tidal field correlations) and Section 5 to the 'II' term (essentially captured by spin–spin correlations).

Before presenting those results, we also give here some guidelines on the way projected correlation functions are worked out in the simulation. In Section 2.2.2, we presented our method for relating three-dimensional galaxy spins $\boldsymbol{L}$ to projected ellipticities in the plane of the sky. It is based on the ansatz that the axis ratio of our galaxies is well approximated by $q = |L_z|/|\boldsymbol{L}|$, where z is the line of sight direction. The orientation of the major axis of the projected ellipse is $\psi = \pi/2 - \arctan(L_y/L_x)$. The projected ellipticities can easily be mapped from Cartesian (1,2) coordinates to the ($+,\times$) frame attached to the separation of a given galaxy pair according to the geometric transformation:

$$e_+ = -e_1\cos(2\beta) - e_2\sin(2\beta), \quad (11)$$

$$e_\times = \quad e_1\sin(2\beta) - e_2\cos(2\beta), \quad (12)$$

where β is the angle between the separation and the first Cartesian coordinate.

With those prescriptions, we can estimate the projected correlation functions for a given projected separation θ. For the II component (dropping the subscript s), this reads

$$\xi_+^{\mathrm{II}}(\theta) = \langle e_+e_+' + e_\times e_\times'\rangle. \quad (13)$$

Beyond this 2D measurement, and to limit the dilution of the IA signal with projected angular distances, we will also measure the correlation as a function of the 3D comoving galaxy separation whilst still considering 2D ellipticities as the result of the projection

[3] Simplified to a flat Universe case.

along a specific line of sight. We call this correlation function $\eta(r)$ following the notations of Heymans et al. (2006) and Joachimi et al. (2013b):

$$\eta(r) = \langle e_+(\boldsymbol{x})e_+(\boldsymbol{x}+\boldsymbol{r}) + e_\times(\boldsymbol{x})e_\times(\boldsymbol{x}+\boldsymbol{r})\rangle_x, \quad (14)$$

where $\boldsymbol{r}$ is the 3D galaxy pair separation.

4 SPIN–TIDAL TENSOR CORRELATIONS

In the context of weak lensing surveys, IA can occur through correlations between the shear induced by the gravitational potential in the lens plane, and the intrinsic ellipticity of galaxies in the source plane. Here, we aim to assess the extent to which the tidal tensor and the galactic spins correlate in the HORIZON-AGN simulation described in Section 2. For this purpose, we first measure in Section 4.1 the one-point correlation between the spins and the tidal tensor. Then, Section 4.2 is devoted to the measurements of the two-point correlations between the spins and the tidal tensor as a function of the separation.

To study the correlations between the spin direction and the surrounding gravitational tidal field of the galaxies resolved in the HORIZON-AGN simulation, we measure the components of the 3D (traceless) tidal shear tensor defined as

$$T_{ij} = \partial_{ij}\Phi - \frac{1}{3}\Delta\Phi\,\delta_{ij}, \quad (15)$$

where Φ is the gravitational potential and δ_{ij} the Kronecker δ function. The minor, intermediate and major eigendirections of the tidal tensor T_{ij} are called $\boldsymbol{e}_1$, $\boldsymbol{e}_2$ and $\boldsymbol{e}_3$ corresponding to the ordered eigenvalues $\lambda_1 \leq \lambda_2 \leq \lambda_3$ of the Hessian of the gravitational potential, $\partial_{ij}\Phi$ (with which the tidal tensor shares the eigendirections). In the filamentary regions, $\boldsymbol{e}_1$ gives the direction of the filament (see Fig. 1), while the walls are collapsing along $\boldsymbol{e}_3$ and extend, locally, in the plane spanned by $\boldsymbol{e}_1$ and $\boldsymbol{e}_2$ (Pogosyan, Bond & Kofman 1998).

The tidal shear tensor smoothed on scale R_s, $T_{ij} = \partial_{ij}\Phi_{R_s} - \Delta\Phi_{R_s}\,\delta_{ij}/3$, is computed via fast Fourier transform of the density field (including DM, stars, gas and BHs) sampled on a 512^3 Cartesian grid and convolved with a Gaussian filter of comoving scale $R_s = 200\,h^{-1}$ kpc:

$$\partial_{ij}\Phi_{R_s}(\boldsymbol{x}) = \frac{3H_0^2\Omega_0}{2a}\int \mathrm{d}^3\boldsymbol{k}\;\delta(\boldsymbol{k})\frac{k_i k_j}{k^2}W_G(kR_s)\exp(\mathrm{i}\,\boldsymbol{k}\cdot\boldsymbol{x}),$$

where $\delta(\boldsymbol{k})$ is the Fourier transform of the sampled density field and W_G a Gaussian filter.

4.1 One-point cross-correlations

We begin with a measurement of the correlations between the spin and the eigendirections of the tidal tensor at the same spatial position. In practice, we compute the cosine of the angle between the spin of the galaxies and the three eigendirections of the local tidal tensor $\cos\theta = \boldsymbol{L}\cdot\boldsymbol{e}_i/|\boldsymbol{L}|$. The resulting histogram is shown in Fig. 3. The spin is preferentially aligned with the minor eigendirection (i.e. the filaments) in agreement with the spin–filament correlations detected by Dubois et al. (2014) at redshift $z \sim 1.83$. To a lower extent, some alignment is found with the direction of the intermediate axis.

When galaxies are binned in mass (see Fig. 4), it appears that the most massive galaxies tend to have a spin lying in the plane $(\boldsymbol{e}_2, \boldsymbol{e}_3)$ perpendicular to the filaments, while the less massive galaxies have their spin aligned with $\boldsymbol{e}_1$. The transition occurs at stellar masses

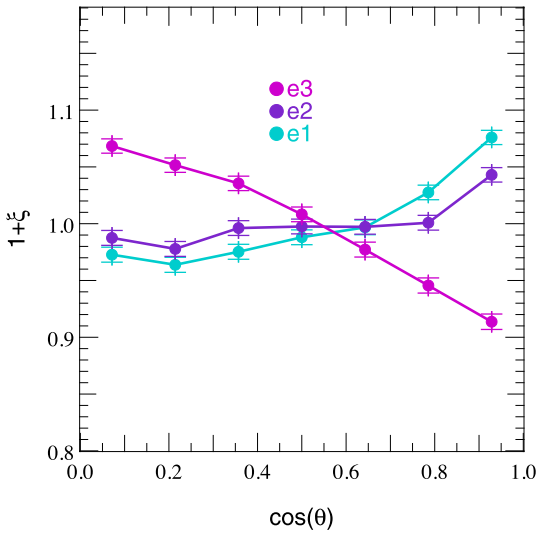

Figure 3. Excess probability of alignment between the spin of galaxies and the minor, intermediate or major axis (respectively cyan, purple and magenta) of the tidal tensor in the HORIZON-AGN simulation. The error bars represent the Poisson noise. The spin of galaxies tends to align with the minor eigendirection. Figs 4 and 5 investigate how this alignment changes with, respectively, galactic mass and colour.

about $4\times10^{10}\,\mathrm{M}_\odot$. We conclude that the spins of *galaxies* are definitely influenced by their surrounding environment differentially with their mass.

Those findings follow very closely what can be found for DM haloes, as detailed in Appendix A where a similar analysis for the alignment of the spin of the DM haloes with the local tidal tensor is carried out. Fig. A1 clearly exhibits the same qualitative correlation as galaxies, namely a transition at a halo mass $\sim5\times10^{11}\,\mathrm{M}_\odot$ from spins aligned with $\boldsymbol{e}_1$, at low mass, to spins oriented in the plane $(\boldsymbol{e}_2, \boldsymbol{e}_3)$ at high mass. This is consistent with previous works based on pure DM simulations (Aragón-Calvo et al. 2007; Hahn et al. 2007a; Paz et al. 2008; Zhang et al. 2009; Codis et al. 2012; Aragón-Calvo 2013; Libeskind et al. 2013, see in particular fig. 3 in Codis et al. 2012).

The colour of galaxies is a quantity more readily accessible to observations. It is therefore of interest to see how different galaxy colours implies different IA as it would provide means on how to leverage this effect. Fig. 5 displays the correlations between galactic spins, and the tidal field for different colours as labelled (see Section 2.2.3 for details about the extraction of galactic colours). The width of the colour bins has been chosen such that there is the same number of objects in each subset of galaxies. On average, the bluest galaxies (defined here by $u - r < 0.78$) are more correlated with the tidal eigendirections than the red galaxies ($u - r > 1.1$ here). This can be easily understood from the fact that red galaxies are typically massive, while blue galaxies are often small-mass galaxies. At that redshift ($z \sim 1.2$), this implies that red galaxies correspond to objects around the transition mass, whereas blue galaxies are mostly aligned with $\boldsymbol{e}_1$. At lower redshift, we expect the population of massive galaxies perpendicular to $\boldsymbol{e}_1$ to increase, so that red galaxies become more correlated. Obviously, we should also keep in mind that applying additional selection cuts on the galaxy samples (mass, luminosity, etc.) would change the level of correlation. For instance, red galaxies above $4\times10^{10}\,\mathrm{M}_\odot$ are more correlated than the whole population of red galaxies.

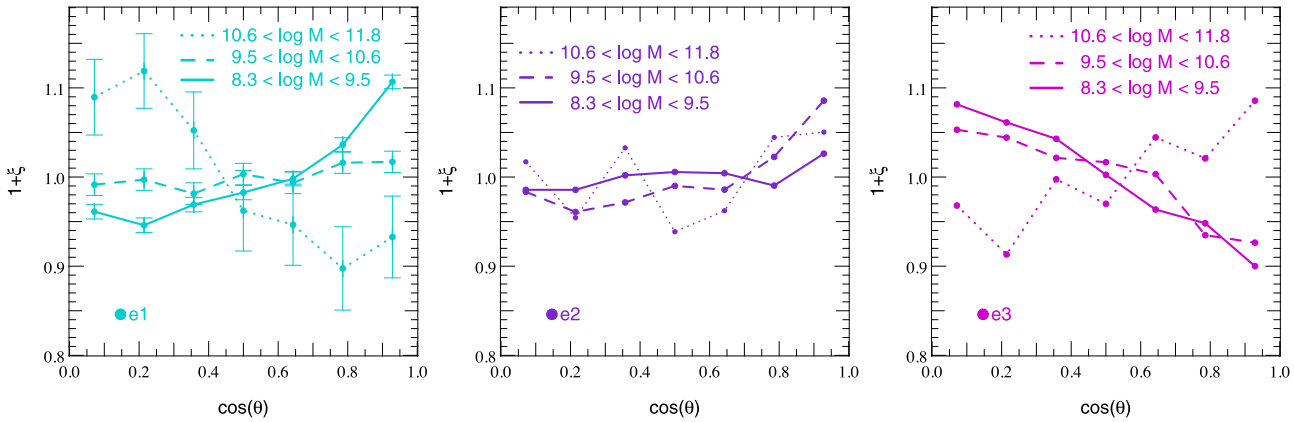

Figure 4. PDF of the cosine of the angle between the spin of galaxies and the minor/intermediate/major axis (from left to right) of the tidal tensor in the HORIZON-AGN simulation when the sample is separated into three different mass bins (solid lines for stellar mass between 2×10^8 and 3×10^9 $M_\odot$, dashed lines for stellar mass between 3×10^9 and 4×10^{10} $M_\odot$ and dotted lines for stellar mass between 4×10^{10} and 6×10^{11} $M_\odot$). The error bars represent the Poisson noise and are only shown for $\boldsymbol{e}_1$ (left-hand panel) since they are the same for $\boldsymbol{e}_2$ (middle panel) and $\boldsymbol{e}_3$ (right-hand panel). The spin of galaxies tends to align with the minor eigendirection at small mass and becomes perpendicular to it at larger mass.

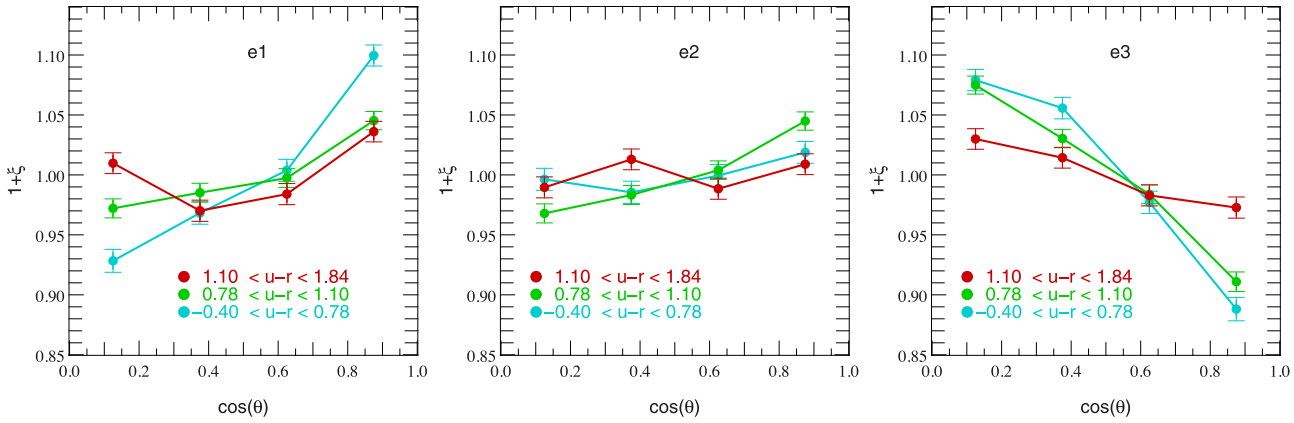

Figure 5. Same as Fig. 4 but for different galaxy colours as labelled, meaning that the left-hand, middle and right-hand panels, respectively, show the PDF of the angle between the $\boldsymbol{e}_1$, $\boldsymbol{e}_2$ and $\boldsymbol{e}_3$ directions of the tidal tensor and the galactic spins. The bluer the galaxy, the larger the correlations with the surrounding tidal field. Hence red galaxies are less sensitive to IA.

4.2 Two-point cross-correlations

While the aforementioned measurements have been performed at the same spatial location, it is also of interest in the context of weak lensing studies to quantify how this signal pervades when the separation between galaxies increases. Because the tidal field in the vicinity of a galaxy contributes also to the lensing signal carried by more distant galaxies, it is clear that the spin—-tidal tensor cross-correlation is closely related to the so-called GI term in the weak lensing terminology. To address that question, we measure the correlations between the spins and the eigendirections of the tidal tensor at comoving distance r. In practice, we compute for each pair of galaxies–grid cell (the tidal field being sampled on a 512^3 Cartesian grid) their relative separation and the angle between the spin of the galaxy and the three eigendirections of the tidal tensor in the corresponding grid cell. We finally do a histogram of these quantities. The results are shown in Fig. 6, which displays the PDF of the cosine of the angle between the spins and $\boldsymbol{e}_1$, $\boldsymbol{e}_2$, $\boldsymbol{e}_3$ as a function of the separation, and Fig. 7, which shows on the same plot the mean angle with $\boldsymbol{e}_1$ (cyan), $\boldsymbol{e}_2$ (purple) and $\boldsymbol{e}_3$ (magenta). As expected, the spin and the tidal eigendirections de-correlate with increasing separation. However, whereas the signal vanishes on scales $r > 3\,h^{-1}$ Mpc for the spin to intermediate tidal eigendirection correlation, it persists on distances as large as $\sim 10\,h^{-1}$ Mpc for the minor and major eigendirections of the tidal tensor.

5 SPIN–SPIN AUTOCORRELATIONS

In the previous section, we focused on the correlations between the spins and the tidal tensor eigendirections as it is related to the 'GI term' which is induced by correlations between the ellipticities and the cosmic shear. We will now investigate the second source of IA that comes from the autocorrelations of the intrinsic ellipticities of galaxies. For that purpose, we study first the spin–spin two-point correlation as a function of the galaxy pair separation (Section 5.1), before turning to the projected ellipticity two-point correlation function (Section 5.2).

5.1 3D spin–spin autocorrelations

We begin with the autocorrelation of the direction of the spins as a function of the galaxy pair separation (in other words, the mean angle between the spin of two galaxies separated by a distance r). We select galaxies of different stellar masses: $2 \times 10^8 < M_s < 3 \times 10^9$, $3 \times 10^9 < M_s < 4 \times 10^{10}$ and $M_s > 4 \times 10^{10}$ $M_\odot$ and different

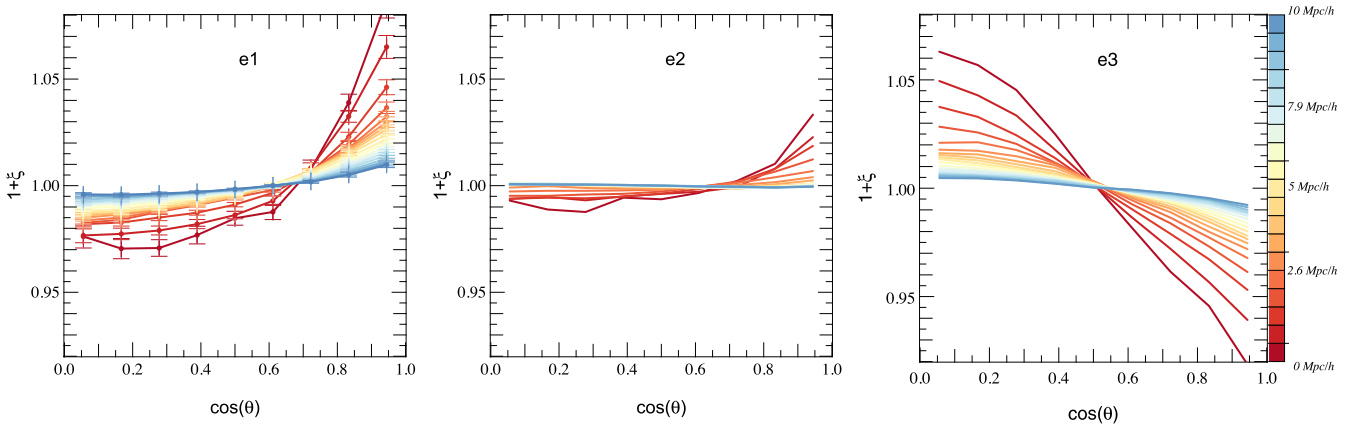

Figure 6. PDF of the cosine of the angle between the spin of galaxies and the tidal tensor (smoothed on 0.4 h^{-1} Mpc) eigendirections $\boldsymbol{e}_1$ (left-hand panel), $\boldsymbol{e}_2$(middle panel) and $\boldsymbol{e}_3$ (right-hand panel) at two locations separated by $r < 10\,h^{-1}$ Mpc (comoving), the separation being colour coded from red to blue. For the sake of readability, the 1σ error on the mean estimating from 32 random resamples is displayed only on the left-hand panel. The spins are more likely to be aligned with $\boldsymbol{e}_1$ and to a lesser extent with $\boldsymbol{e}_2$ at short distance in agreement with the one-point PDF shown in Fig. 3; this signal decreases when the separation increases as expected. This de-correlation is faster for $\boldsymbol{e}_2$ than for the other two eigendirections, going from a few to 10 h^{-1} Mpc.

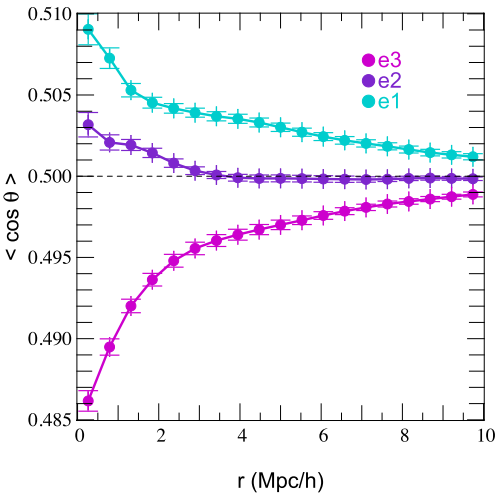

Figure 7. Mean angle between the spin and the tidal eigendirections as a function of the separation. Error bars represent the 1σ error on the mean when cutting the statistics into 32 subsets. The spins are aligned with the minor direction (cyan) and to some extent with the intermediate eigendirection (purple) at small distance and decorrelate on different scales. The alignment with $\boldsymbol{e}_1$ and $\boldsymbol{e}_3$ pervade on scales of about 10 h^{-1} Mpc but is reduced to $\sim$3 h^{-1} Mpc for the intermediate direction.

colours. For each pair of such galaxies separated by a comoving distance r, we measure the angle between their respective spin, and compute the square of the cosine of this angle, $\cos^2\alpha$ (as the polarity is of no interest for weak lensing), in Fig. 8. Error bars represent the error on the mean $\sqrt{\langle\cos^4\theta\rangle - \langle\cos^2\theta\rangle^2/N}$.

We do not detect any significant spin correlation either among red galaxies or between red and blue galaxies. Conversely we measure a significant spin correlation for blue galaxies out to at least a comoving distance of 10 h^{-1} Mpc. We also see that the correlation amplitude is strong for low- and intermediate-mass galaxies. The signal for the most massive galaxies or red galaxies is compatible with zero correlation at any distance. The importance of grid locking on these correlation is estimated in Section 6 where it is shown that it is not significant.

5.2 2D ellipticity–ellipticity correlations

The two quantities $\xi_+^{\rm II}$ and $\eta(r)$ defined in Section 3 are measured on our synthetic data and shown in Fig. 9. The panels in the top row show our findings for $\eta(r)$ for three populations of galaxies where we choose a direction [here (0.34, 0.06, 0.94) in Cartesian coordinates] in the box different from the grid as the line of sight. Like the previous 3D analysis, there is a striking difference of behaviour between red and blue galaxies, the latter showing a strong correlation signal for the statistics of η with a typical amplitude of $\sim 3 \times 10^{-3}$ between 1 and 5 h^{-1} Mpc. On the other hand, the correlation for red galaxies is compatible with zero. We can therefore anticipate that blue galaxies at redshift $\sim$1.2 should be affected by IA, leaving the possibility of a substantial contamination of the weak lensing signal. The bottom panels of Fig. 9 show the amplitude of the correlation function $\xi_+^{\rm II}(\theta)$ as a function of the angular galaxy pairs separation.[4] It is significant and comparable to the cosmic shear amplitude all the way to $\sim$13 arcmin.

Let us now compare our findings to the recent study of Joachimi et al. (2013b), which is based on a semi-analytical model of galaxy formation. At first glance, we draw opposite conclusions, as we measure a strong level of IA for blue galaxies and no noticeable signal for red galaxies, whereas Joachimi et al. predict a strong alignment of red galaxies ($\eta \sim 10^{-2}$ at $z = 1.5$ and $r = 1\,h^{-1}$ Mpc) and a low level of alignment of blue galaxies ($\lesssim 3 \times 10^{-4}$ at $r = 1\,h^{-1}$ Mpc, compatible with zero correlation). Yet, several important differences should be emphasized.

(i) All our galaxies are assumed to be thin discs with a value $q_{\rm d} = 0$ in equation (4) whereas Joachimi et al. explore two values $q_{\rm d} = 0.1$ and 0.25 for late-type galaxies. Recall that our choice of $q_{\rm d} = 0$ will tend to maximize the amplitude of projected ellipticities. We repeated the measurement of $\xi_+^{\rm II}$ assuming a value of $q_{\rm d} = 0.25$ which assumes quite a strong thickening of the disc. The net result shown in Fig. 10 is to decrease the normalization of $\xi_+^{\rm II}$ for blue galaxies by a factor of $\sim$3, to a typical amplitude of $\xi_+^{\rm II} \simeq 2 \times 10^{-4}$

[4] Note that a $1\,h^{-1}$ Mpc comoving transverse distance corresponds to an angular size of 1.3 arcmin at this redshift.

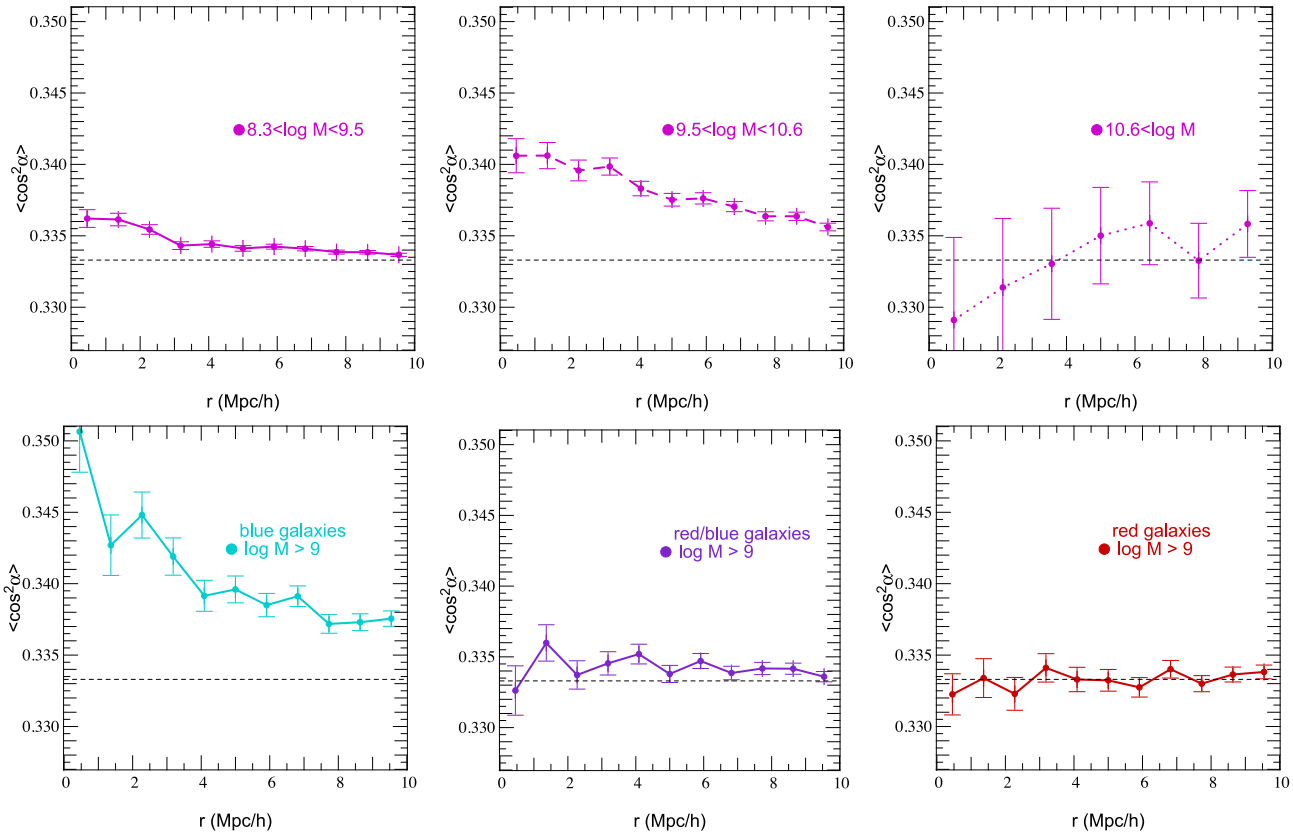

Figure 8. 3D spin–spin two-point correlation function of galaxy as a function of the comoving separation for a range of stellar masses: $2 \times 10^8 < M_s < 3 \times 10^9\,M_\odot$ (top left-hand panel), $3 \times 10^9 < M_s < 4 \times 10^{10}\,M_\odot$ (top centre panel) and $M_s > 4 \times 10^{10}\,M_\odot$ (top right-hand panel), or colours: blue galaxies, i.e. $u - r < 0.78$ (bottom left-hand panel), red galaxies, i.e. $u - r > 1.1$ (bottom right-hand panel) and the cross-correlations between blue and red galaxies (bottom centre panel). Note that for blue and red galaxies we also apply a mass cut below $10^9\,M_\odot$ (i.e. 300 star particles). Error bars represent the error on the mean. Here we choose to display the mean square cosine between two spins (separated by the comoving distance r) as the polarity is not relevant to weak lensing studies. For a uniform random distribution, the expectation is 1/3 (dashed line). Blue galaxies and small-to-middle mass galaxies are indeed correlated on the scale of the typical size of filaments, $\gtrsim 10\,h^{-1}$ Mpc, whereas red and high-mass galaxies do not show a significant correlation.

between 1 and 5 h^{-1} Mpc at $z \sim 1.2$ (but for intermediate-mass galaxies, the amplitude of the correlation remains qualitatively the same).

(ii) Our distinction of red and blue galaxies may not correspond exactly to their early- and late-type classification. For instance, our red galaxies sample is dominated by low-mass red satellite instead of massive red central galaxies. But this effect cannot fully explain the difference.

(iii) To assign a spin to their late-type galaxies (somehow equivalent to our blue sample), Joachimi et al. used the results of Bett (2012) for the alignment between the DM halo spin orientation and the galaxy spin at redshift zero. These were obtained with several hydrodynamical zoom simulations in a $\sim$12.5 or $\sim 20\,h^{-1}$ Mpc size volume. As shown in Fig. A2, we find at redshift $z \sim 1.2$ a somewhat weaker alignment between galaxy and halo spins than Bett (2012). Naively, this fact should produce weaker two-point galaxy spin–spin correlation than the Joachimi et al. results. However, Dubois et al. (2014) showed that the spin of galaxies are in fact as correlated with the large-scale filaments as their DM host halo. This is a consequence of cold flows that advect efficiently the cosmic angular momentum all the way to galaxies at the centre of dark haloes (Kimm et al. 2011; Pichon et al. 2011; Danovich et al. 2012; Stewart et al. 2013). Therefore semi-analytic models, which chain the de-correlation between the large-scale structure and the halo, and that between the halo and the disc galaxies, will most certainly underestimate the correlation of these galaxies with the large-scale structure.

(iv) Conversely, the most likely explanation for the discrepancy of the red population is twofold. First, the red galaxies here are objects around the transition mass. Hence, part of them have their spin aligned with the surrounding filament (below the transition mass), while the others have their spin perpendicular to it (above the transition mass). Therefore, on average no correlation is detected among that sample. Nevertheless, for larger mass and lower redshift, this population is expected to become more strongly perpendicular to the filaments and thus more correlated. Again, one should bear in mind that any selection (mass, colour, luminosity, etc.) may bias significantly the two-point ellipticity correlations. Second, spins alone may not fully capture the shape of non-rotating, mostly triaxial early-type galaxies. We defer for future work a thorough analysis of ellipticity alignments with the inertia tensor of galaxies as a proxy for ellipticity.

Note finally that the coherence of the large-scale structure is expected to be higher with increasing redshift. We may therefore speculate that, at later times, the intrinsic correlation of spins will decrease (see also Lee et al. 2008; Joachimi et al. 2013b).

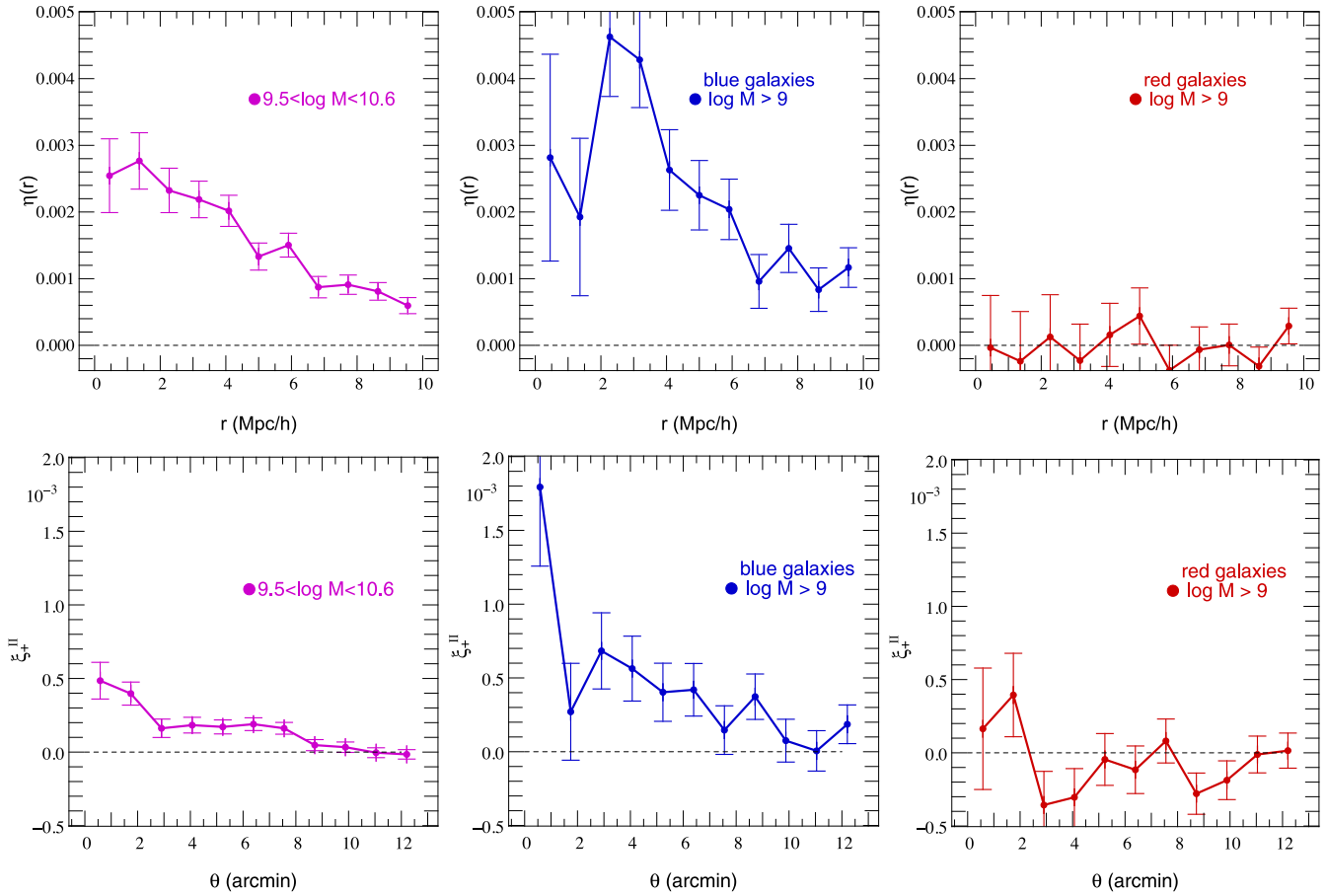

Figure 9. Correlation functions of the projected ellipticity $\eta(r)$ for the ∼58 000 middle-mass (left-hand panels), ∼25 000 blue (middle panels) and ∼25 000 red (right-hand panels) galaxies as a function of the comoving 3D separation r, in the top row, and as a function of the (projected) angular separation θ in the bottom row; this latter quantity being closer to observations, we call it $\xi_+^{\rm II}$. Note the change in scale from one row to the other and the additional mass cut below $10^9\,{\rm M}_\odot$ (i.e. 300 star particles).

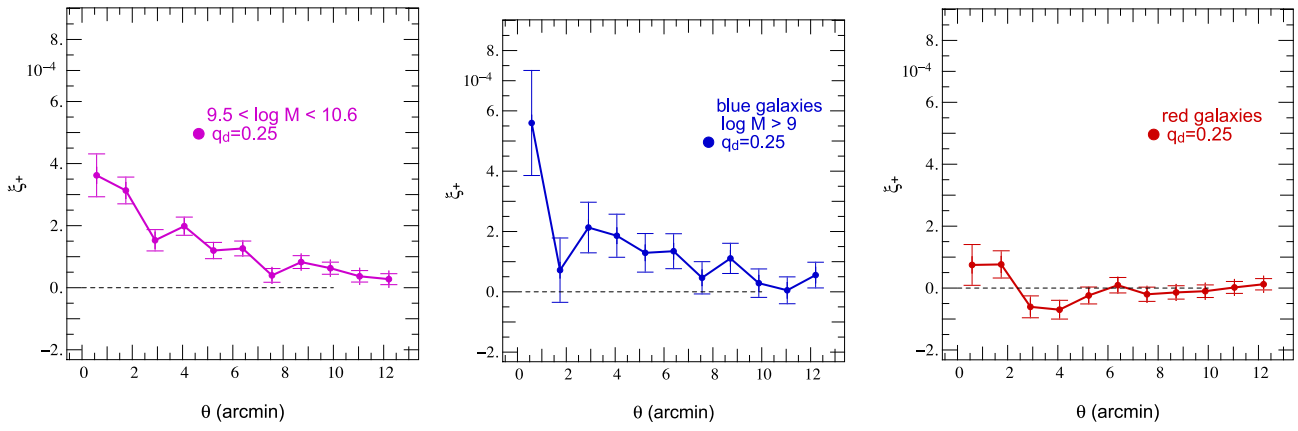

Figure 10. Same as bottom panels of Fig. 9 for thicker discs $q_{\rm d} = 0.25$.

6 GRID LOCKING EFFECT ON SPIN ALIGNMENTS

Grid locking effects are a concern for spin–spin correlation functions when using grid-based codes such as AMR (see also Dubois et al. 2014 for details about how spins are correlated with the Cartesian grid). The alignments of the spins with the grid are shown in Fig 11. To investigate this effect on the two-point statistics studied in this work, we compute the same statistics (spin–spin correlation functions and its 2D counterpart, $\xi_+^{\rm II}$) after a random permutation of the spins in the box. This allows us to keep the same one-point distribution of spins on the sphere, including the corresponding level of grid locking, but to remove the physical two-point correlations (the box size being much larger than the typical correlation length). Thus any signal in the data, relative to the random permutation of spins, should be physical and not induced by grid locking. Fig. 12

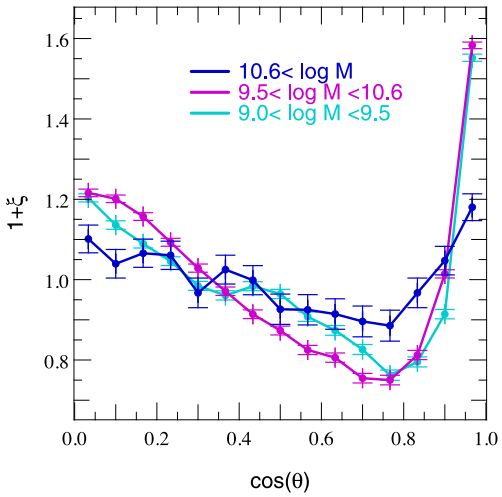

Figure 11. Excess probability of alignment, ξ, between the spins and the grid axes for different bins of mass. The most massive galaxies (blue solid line) are the least prone to grid locking. Note that the displayed plot is the mean on the PDF obtained for the x, y and z axes.

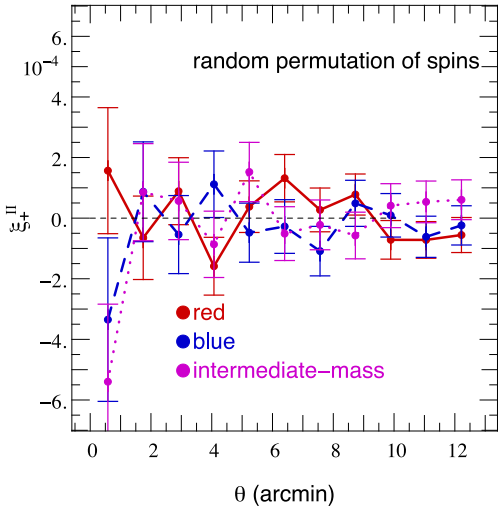

Figure 12. $\xi_+^{\rm II}$, the two-point projected ellipticity correlation function for intermediate-mass, blue and red galaxies when spins are randomly swapped in the box. The three panels are statistically compatible with non-correlation, meaning that grid locking does not introduce significant ellipticity correlations. This allows us to assume that the correlations detected in Fig. 9 are physical and not due to grid locking effects.

shows the result for different populations of galaxies (blue, red and intermediate mass). It appears that all those correlations are consistent with $\xi_+^{\rm II} = 0$, implying that the results presented in the main text (e.g. Fig. 9) are not significantly biased by grid locking. The same conclusion holds for spin–spin correlations and $\eta(r)$.

To be more precise, let us assume that the spin of a galaxy in the simulation is the superposition of the 'real' spin plus a numerical contribution coming from grid locking $\boldsymbol{s} = \boldsymbol{s}_{\rm s} + \boldsymbol{s}_{\rm gl}$ where we neglect normalizations (all spins are of norm 1 here). Then the two-point function of the measured spin of galaxies reads

$$\langle \boldsymbol{s}(\boldsymbol{x})\boldsymbol{s}(\boldsymbol{x}+\boldsymbol{r})\rangle = \langle \boldsymbol{s}_{\rm s}(\boldsymbol{x})\boldsymbol{s}_{\rm s}(\boldsymbol{x}+\boldsymbol{r})\rangle + 2\left\langle \boldsymbol{s}_{\rm s}(\boldsymbol{x})\boldsymbol{s}_{\rm gl}(\boldsymbol{x}+\boldsymbol{r})\right\rangle + \left\langle \boldsymbol{s}_{\rm gl}(\boldsymbol{x})\boldsymbol{s}_{\rm gl}(\boldsymbol{x}+\boldsymbol{r})\right\rangle . \quad (16)$$

Let us also assume that the spin contributions coming from grid locking do not depend on spatial location. Then $\left\langle \boldsymbol{s}_{\rm s}(\boldsymbol{x})\boldsymbol{s}_{\rm gl}(\boldsymbol{x}+\boldsymbol{r})\right\rangle$ and $\left\langle \boldsymbol{s}_{\rm gl}(\boldsymbol{x})\boldsymbol{s}_{\rm gl}(\boldsymbol{x}+\boldsymbol{r})\right\rangle$ do not depend on $\boldsymbol{r}$, i.e. those terms are constant. Therefore one can write

$$\langle \boldsymbol{s}(\boldsymbol{x})\boldsymbol{s}(\boldsymbol{x}+\boldsymbol{r})\rangle = \langle \boldsymbol{s}_{\rm s}(\boldsymbol{x})\boldsymbol{s}_{\rm s}(\boldsymbol{x}+\boldsymbol{r})\rangle + C. \quad (17)$$

If one permutes all the spins in the box the physical two-point correlation of spins $\langle \boldsymbol{s}_{\rm s}(\boldsymbol{x})\boldsymbol{s}_{\rm s}(\boldsymbol{x}+\boldsymbol{r})\rangle$ goes to zero if the box is large enough and C remains C as it does not depend on the spatial coordinates. We therefore measured this term in the simulation and found that $|C| \lesssim 10^{-4}$, which is below the statistical uncertainties currently plaguing our physical measurements. If grid locking does not depend on spatial location, we can conclude that the measured spin–spin correlation function is not significantly biased.

Another test that one can perform is to restrict the analysis to the galaxies that are less grid locked. We therefore measured the spin–spin correlation function for the most massive galaxies (that were shown to be the least sensitive to grid locking in Fig. 11). The result is displayed in Fig. 13. As the signal remains qualitatively the same (the amplitude is even larger), we conclude that grid locking cannot be the main source of spin correlations measured in the simulation. Note that this test does not make any assumption on the physical origin of grid locking.

The only way to go beyond the tests proposed in this section would be to compare our results with similar cosmological hydrodynamics simulations performed using a technique which does not suffer from grid locking, but this is clearly beyond the scope of this paper.

7 SUMMARY AND CONCLUSION

Using the HORIZON-AGN simulation, we have shown that low-mass galaxies tend to have their spin aligned with the local tidal field minor eigendirection (the filamentary direction), whereas more massive galaxies ($M_{\rm s} > 4 \times 10^{10}\,{\rm M}_\odot$ at redshift one) have their spin mostly aligned with the major tidal eigendirection (i.e. perpendicular to walls and filaments). The corresponding two-point correlation decreases with the comoving separation out to scales as large as $\sim 10\,h^{-1}$ Mpc, with a faster de-correlation for the spin-to-the-intermediate-axis direction ($\sim 3\,h^{-1}$ Mpc), a result consistent with Lagrangian theory in this context (Codis et al., in preparation). Those results depend on the properties of galaxies, in particular on their mass and intrinsic colour. For instance, it was clearly found that at $z \simeq 1.2$ in the HORIZON-AGN simulation, blue galaxies and intermediate-mass galaxies are significantly correlated with the gravitational tidal field whereas red and massive galaxies do not show any correlations. We reach identical conclusions when studying the alignment of galaxy spins with one another, namely that the spins of galaxies are also correlated on similar scales ($\sim 10\,h^{-1}$ Mpc) and are similarly colour and mass dependent.

We have also investigated how spin–spin correlations project into weak lensing observables like the shear correlation function ξ_+, these correlations being cast into the so-called II contributions to IA. As in 3D, a $\xi_+^{\rm II}$ correlation at a level of a few 10^{-4} is found for blue and intermediate-mass galaxies out to separations of $\gtrsim 10$ arcmin for sources at redshift $\sim$1.2. The results for blue galaxies are in broad agreement with the recent work of Joachimi et al. (2013b), who combine observational results on IA from the Cosmic Evolution Survey (COSMOS) and predictions from semi-analytical models applied to DM-only simulations. The effect of grid locking on the two-point functions was shown to be subdominant. However,

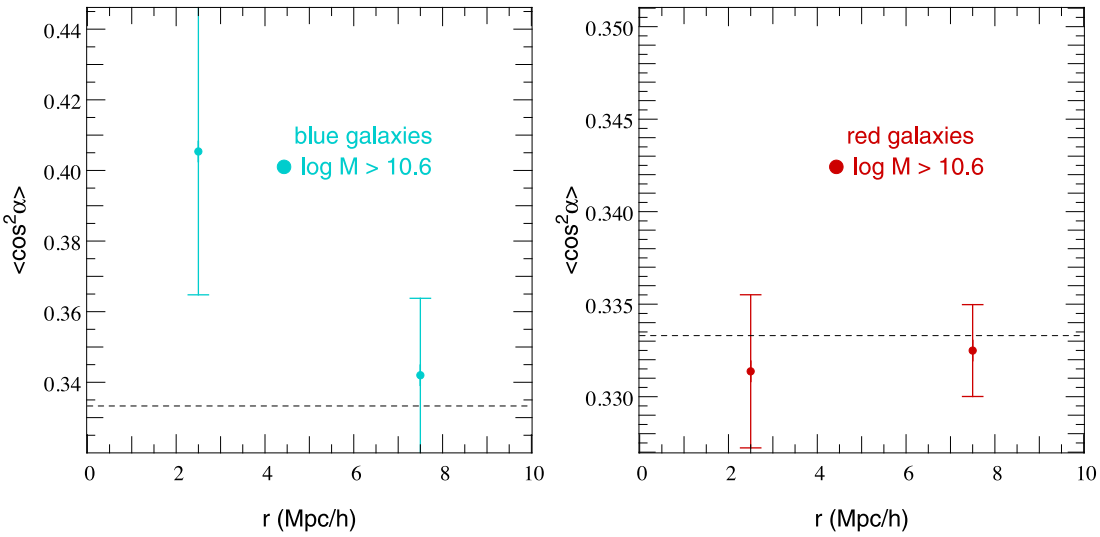

Figure 13. 3D spin–spin two-point correlation function of galaxy as a function of the comoving separation for blue galaxies, i.e. $u - r < 0.78$ (left-hand panel) and red galaxies, i.e. $u - r > 1.1$ (right-hand panel) with a mass cut below $4 \times 10^{10}\,\mathrm{M}_{\odot}$. Same qualitative results as in Fig. 8 are found. Hence, grid locking should not be the dominant source of the observed spin correlations.

to go beyond this qualitative statement and accurately quantify the effect of grid locking, one would need to perform a similar simulation using a numerical technique insensitive to this specific systematic error, such as smoothed particle hydrodynamics (SPH) or unstructured mesh.

Presently, the 'spin-gives-ellipticity' prescription allows one to quantify the new insights that large volume hydrodynamical cosmological simulations bring to the issue of IA. For instance, the large-scale coherence of gas motions advected all the way to the centre of galaxies through cold flows regardless of the DM behaviour can uniquely be captured by such simulations (Kimm et al. 2011). Large-scale dynamics imprint their coherence and morphology (filaments, walls, voids) on to the spin of galaxies. This complex topology is likely to have an even more prominent impact on higher order statistics beyond the shear two-point correlation function. Attempts to capture such effects with simple halo occupancy distribution prescriptions may therefore fail at high redshift ($z \gtrsim 0.8$), which is the place where galaxies carry more cosmological lensing signal and is also, to large extent, the population of sources targeted by future surveys like *Euclid* or LSST. The challenge for simulations is to cover large cosmological volumes while preserving a sufficient resolution so that baryonic physics (star formation, feedback processes, etc.) is correctly treated.

When the HORIZON-AGN simulation reaches redshift zero, we will be in a good position to compare our findings with existing observations. In order to get a good match for massive red galaxies, we will certainly adopt a different ansatz for our recipe – currently based on a thin disc approximation – and use directly the resolved shape of massive galaxies as a proxy for the projected ellipticities. However, this concerns only a small fraction of the galaxies that made up the typical weak lensing catalogues of background sources. Once the HORIZON-AGN light-cone is completed, we will estimate more realistic galactic shapes, taking full account of the spectral energy distribution of young and old stars (giving a non-trivial weight to the relative contribution of the disc and the bulge) into a well chosen rest-frame filter (e.g. using the broad *Euclid* VIS band), and more precisely mimicking observational selection effects (i.e. a flux-limited sample of background sources will capture specific populations of sources at a given redshift). This will allow us to quantify the amount of contamination from IA expected in real surveys, and possibly mitigate their nuisance by selecting galaxies that are less prone to IA based on colour.

ACKNOWLEDGEMENTS

This work has made use of the HPC resources of CINES (Jade supercomputer) under the allocation 2013047012 and 2014047012 made by GENCI. Part of the analysis was performed on the DiRAC facility jointly funded by STFC and the Large Facilities Capital Fund of BIS. This work is partially supported by the Spin(e) grants ANR-13-BS05-0005 of the French *Agence Nationale de la Recherche* and by the ILP LABEX (under reference ANR-10-LABX-63 and ANR-11-IDEX-0004-02). The research of YD has been supported at IAP by ERC project 267117 (DARK) hosted by Université Pierre et Marie Curie – Paris 6. We thank S. Rouberol for running smoothly the HORIZON cluster for us, and D. Munro for freely distributing his YORICK programming language and OPENGL interface (available at http://yorick.sourceforge.net/). SC and CP thank Lena for her hospitality during the course of this work. VD would like to thank the Institut d'Astrophysique de Paris for hospitality during the completion of this work, and acknowledges support by the Swiss National Science Foundation. JD and ASs research is supported by funding from Adrian Beecroft, the Oxford Martin School and the STFC.

REFERENCES

Aragón-Calvo M. A., 2013, preprint (arXiv:e-prints)
Aragón-Calvo M. A., van de Weygaert R., Jones B. J. T., van der Hulst J. M., 2007, ApJ, 655, L5
Aubert D., Pichon C., Colombi S., 2004, MNRAS, 352, 376
Bailin J., Steinmetz M., 2005, ApJ, 627, 647
Bartelmann M., Schneider P., 2001, Phys. Rep., 340, 291
Bernstein G. M., Norberg P., 2002, AJ, 124, 733
Bett P., 2012, MNRAS, 420, 3303
Bett P., Eke V., Frenk C. S., Jenkins A., Okamoto T., 2010, MNRAS, 404, 1137
Blazek J., Mandelbaum R., Seljak U., Nakajima R., 2012, J. Cosmol. Astropart. Phys., 5, 41
Booth C. M., Schaye J., 2009, MNRAS, 398, 53

Bridle S., King L., 2007, New J. Phys., 9, 444
Brown M. L., Taylor A. N., Hambly N. C., Dye S., 2002, MNRAS, 333, 501
Bruzual G., Charlot S., 2003, MNRAS, 344, 1000
Catelan P., Kamionkowski M., Blandford R. D., 2001, MNRAS, 320, L7
Codis S., Pichon C., Devriendt J., Slyz A., Pogosyan D., Dubois Y., Sousbie T., 2012, MNRAS, 427, 3320
Croft R. A. C., Metzler C. A., 2000, ApJ, 545, 561
Danovich M., Dekel A., Hahn O., Teyssier R., 2012, MNRAS, 422, 1732
Deason A. J. et al., 2011, MNRAS, 415, 2607
Dubois Y., Teyssier R., 2008, A&A, 477, 79
Dubois Y., Devriendt J., Slyz A., Teyssier R., 2012, MNRAS, 420, 2662
Dubois Y. et al., 2014, MNRAS, 444, 1453
Forero-Romero J. E., Contreras S., Padilla N., 2014, MNRAS, 443, 1090
Greggio L., Renzini A., 1983, A&A, 118, 217
Haardt F., Madau P., 1996, ApJ, 461, 20
Hahn O., Porciani C., Carollo C. M., Dekel A., 2007a, MNRAS, 375, 489
Hahn O., Carollo C. M., Porciani C., Dekel A., 2007b, MNRAS, 381, 41
Hahn O., Teyssier R., Carollo C. M., 2010, MNRAS, 405, 274
Heavens A., Refregier A., Heymans C., 2000, MNRAS, 319, 649
Heymans C., Brown M., Heavens A., Meisenheimer K., Taylor A., Wolf C., 2004, MNRAS, 347, 895
Heymans C., White M., Heavens A., Vale C., van Waerbeke L., 2006, MNRAS, 371, 750
Hirata C. M., Seljak U., 2004, Phys. Rev. D, 70, 063526
Hirata C. M. et al., 2004, MNRAS, 353, 529
Hirata C. M., Mandelbaum R., Ishak M., Seljak U., Nichol R., Pimbblet K. A., Ross N. P., Wake D., 2007, MNRAS, 381, 1197
Joachimi B., Bridle S. L., 2010, A&A, 523, A1
Joachimi B., Schneider P., 2008, A&A, 488, 829
Joachimi B., Schneider P., 2010, A&A, 517, A4
Joachimi B., Mandelbaum R., Abdalla F. B., Bridle S. L., 2011, A&A, 527, A26
Joachimi B., Semboloni E., Bett P. E., Hartlap J., Hilbert S., Hoekstra H., Schneider P., Schrabback T., 2013a, MNRAS, 431, 477
Joachimi B., Semboloni E., Hilbert S., Bett P. E., Hartlap J., Hoekstra H., Schneider P., 2013b, MNRAS, 436, 819
Kennicutt R. C., Jr, 1998, ApJ, 498, 541
Kimm T., Devriendt J., Slyz A., Pichon C., Kassin S. A., Dubois Y., 2011, preprint (arXiv:e-prints)
Kirk D., Bridle S., Schneider M., 2010, MNRAS, 408, 1502
Komatsu E. et al., 2011, ApJS, 192, 18
Krumholz M. R., Tan J. C., 2007, ApJ, 654, 304
Laigle C. et al., 2015, MNRAS, 446, 2744
Laureijs R. et al., 2011, preprint (arXiv:e-prints)
Lee J., Pen U.-L., 2002, ApJ, 567, L111
Lee J., Springel V., Pen U.-L., Lemson G., 2008, MNRAS, 389, 1266
Lee B. et al., 2013, ApJ, 774, 47
Leitherer C. et al., 1999, ApJS, 123, 3
Leitherer C., Ortiz Otálvaro P. A., Bresolin F., Kudritzki R.-P., Lo Faro B., Pauldrach A. W. A., Pettini M., Rix S. A., 2010, ApJS, 189, 309
Libeskind N. I., Hoffman Y., Forero-Romero J., Gottlöber S., Knebe A., Steinmetz M., Klypin A., 2013, MNRAS, 428, 2489
Mandelbaum R., Hirata C. M., Ishak M., Seljak U., Brinkmann J., 2006, MNRAS, 367, 611
Mandelbaum R. et al., 2011, MNRAS, 410, 844
Nelson D., Vogelsberger M., Genel S., Sijacki D., Kereš D., Springel V., Hernquist L., 2013, MNRAS, 429, 3353
Paz D. J., Stasyszyn F., Padilla N. D., 2008, MNRAS, 389, 1127
Pichon C., Pogosyan D., Kimm T., Slyz A., Devriendt J., Dubois Y., 2011, MNRAS, 418, 2493
Pichon C., Codis S., Pogosyan D., Dubois Y., Desjacques V., Devriendt J., 2014, arXiv e-prints
Pogosyan D., Bond J. R., Kofman L., 1998, J. R. Astron. Soc. Canada, 92, 313
Porciani C., Dekel A., Hoffman Y., 2002, MNRAS, 332, 325
Rasera Y., Teyssier R., 2006, A&A, 445, 1
Salpeter E. E., 1955, ApJ, 121, 161
Scannapieco C. et al., 2012, MNRAS, 423, 1726
Schneider M. D., Bridle S., 2010, MNRAS, 402, 2127
Schneider P., van Waerbeke L., Kilbinger M., Mellier Y., 2002, A&A, 396, 1
Shakura N. I., Sunyaev R. A., 1973, A&A, 24, 337
Sousbie T., Pichon C., Colombi S., Pogosyan D., 2008, MNRAS, 383, 1655
Stewart K. R., Brooks A. M., Bullock J. S., Maller A. H., Diemand J., Wadsley J., Moustakas L. A., 2013, ApJ, 769, 74
Sutherland R. S., Dopita M. A., 1993, ApJS, 88, 253
Tenneti A., Mandelbaum R., Di Matteo T., Feng Y., Khandai N., 2014, MNRAS, 441, 470
Teyssier R., 2002, A&A, 385, 337
Zhang Y., Yang X., Faltenbacher A., Springel V., Lin W., Wang H., 2009, ApJ, 706, 747

APPENDIX A: DARK MATTER HALOES

Fig. A1 displays the PDF of the cosine of the angle between the tidal eigendirections and the spin of DM haloes of different masses. The same qualitative behaviour as for galaxies is detected: the less massive haloes have a spin preferentially aligned with $\boldsymbol{e}_1$ (somehow

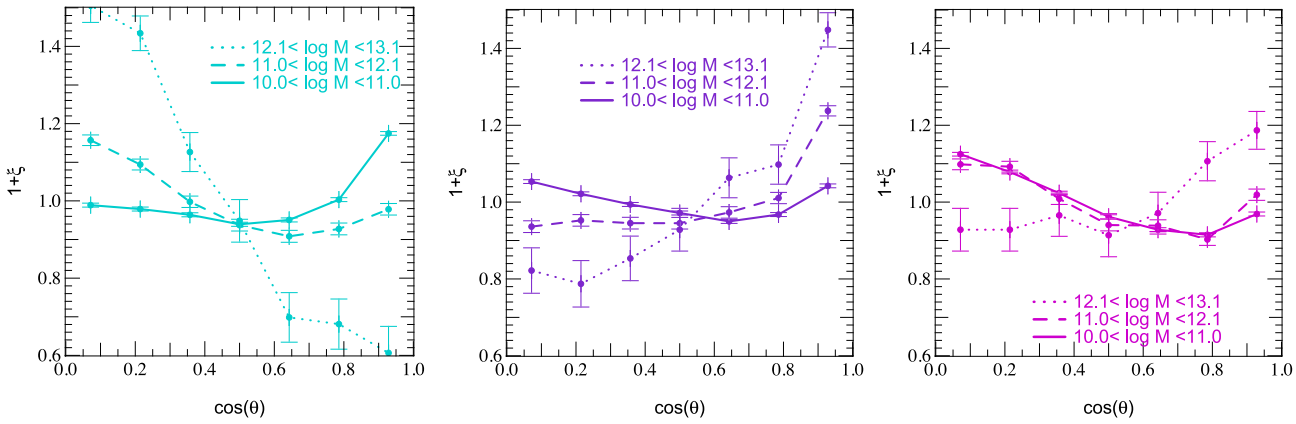

Figure A1. Same as Fig. 3 for DM haloes in the HORIZON-AGN simulation. The three different axes of the tidal tensor are colour coded from cyan ($\boldsymbol{e}_1$) to magenta ($\boldsymbol{e}_3$) through purple ($\boldsymbol{e}_2$). Different mass bins are coded from solid (10^{10}–10^{11} $M_\odot$) to dotted (10^{12}–10^{13} $M_\odot$) through dashed lines (10^{11}–10^{12} $M_\odot$). A transition is detected: the spin of high-mass haloes tends to be aligned with the intermediate (centre purple panel) and with less probability major (right-hand magenta panel) principal axis, whereas the spin of low-mass haloes is more likely to point along the minor axis (left-hand cyan panel). Those findings are consistent with previous studies of DM-only simulations.

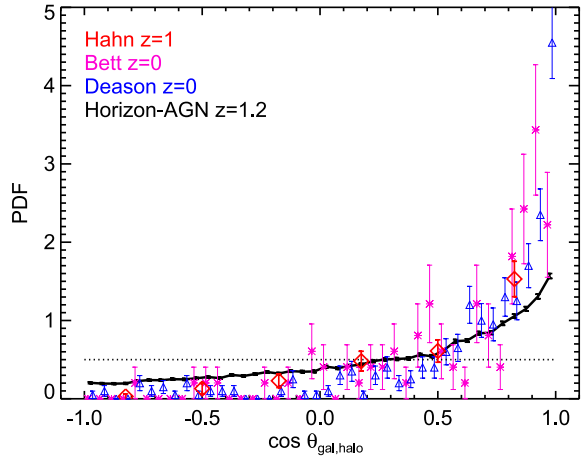

Figure A2. PDF of the cosine of the angle between the spin of the DM halo and that of the galaxy in our simulation at $z = 1.2$ (solid) and from Hahn et al. (2010) at $z = 1$ (red diamonds), from Bett et al. (2010) (pink stars) and from Deason et al. (2011) (blue triangles) both at $z = 0$. The dotted line refers to a uniform isotropic distribution. Error bars are the 1σ standard deviation for Poisson statistics.

the filaments) while higher masses have their spin perpendicular to it (in agreement with what previous studies found in DM-only simulations).

Fig. A2 shows the PDF of the cosine of the angle between the spin of the DM halo and the spin of the galaxy for ∼32 000 pairs at $z = 1.2$ for haloes with virial mass $M_{\rm h} > 10^{11}\,{\rm M}_{\odot}$. We compare our result to that of Hahn et al. (2010) ($z = 1$, $M_{\rm h} > 10^{11}\,{\rm M}_{\odot}$, 89 pairs), Bett et al. (2010) ($z = 0$, $M_{\rm h} > 5 \times 10^{9}\,{\rm M}_{\odot}$, 99 pairs) and Deason et al. (2011) ($z = 0$, $5 \times 10^{11} < M_{\rm h} < 5 \times 10^{12}\,{\rm M}_{\odot}$, 431 pairs). It shows that galaxies are slightly less aligned with their host DM halo in our HORIZON-AGN simulation than what is found by other works, and used in the semi-analytic model of Joachimi et al. (2013b) (based on Bett et al. 2010; Deason et al. 2011), even though all results are compatible within 2σ error bars. This slight difference might originate from AMR (HORIZON-AGN; Hahn et al. 2010) versus SPH (Bett et al. 2010; Deason et al. 2011), the persistence of cold flows (Nelson et al. 2013), disc versus elliptical galaxies (Scannapieco et al. 2012), representativity of their resimulations, etc. Note that both AMR runs (HORIZON-AGN and that of Hahn et al. 2010 performed with the RAMSES code as well) at the same redshift are in better agreement.

This paper has been typeset from a TEX/LATEX file prepared by the author.